

Supporting information

Thiochromenocarbazole Imide: A new organic dye with first utility in large area flexible electroluminescent devices

José María Andrés Castán,^[a] Amruth C,^[b] Pierre Josse,^[a] Laura Abad Galan,^[c] Pablo Simón Marqués,^[a] Magali Allain,^[a] Olivier Maury,^[c] Tangui Le Bahers,^[c] Philippe Blanchard,^[a] Cyrille Monnereau,^{[c]*} Gregory C. Welch^{[b]*} and Clément Cabanetos ^{[a,c]*}

[a] Univ Angers, CNRS, MOLTECH-ANJOU, SFR MATRIX, F-49000 Angers, France

[b] Department of Chemistry, University of Calgary, 731 Campus Place N.W., Calgary, Alberta, Canada

[c] Univ Lyon, ENS de Lyon, CNRS UMR 5182, Université Claude Bernard Lyon 1, F-69342 Lyon, France

[d] Building Blocks for FUTURE Electronics Laboratory (2BFUEL), IRL2002, CdRS -Yonsei University, Seoul, South Korea

E-mail: cyrille.monnereau@ens-lyon.fr, gregory.welch@ucalgary.ca, clement.cabanetos@cnrs.fr

Table of contents

General information

Synthetic procedures

NMR Spectra

HRMS Spectra

Crystallographic data

Optical data

Computed data

Device fabrication and characterization

General information

All reagents and chemicals from commercial sources were used without further purification. Solvents were dried and purified using standard techniques. Flash chromatography was performed with analytical-grade solvents using Aldrich silica gel (technical grade, pore size 60 Å, 230-400 mesh particle size). Flexible plates ALUGRAM® Xtra SIL G UV254 from MACHEREY-NAGEL were used for TLC. Compounds were detected by UV irradiation (Bioblock Scientific). NMR spectra were recorded with a Bruker AVANCE III 300 (¹H, 300 MHz and ¹³C, 75MHz) or a Bruker AVANCE DRX500 (¹H, 500 MHz; ¹³C, 125 MHz). Chemical shifts are given in ppm relative to TMS and coupling constants J in Hz. Matrix Assisted Laser Desorption/Ionization was performed on MALDI-TOF MS BIFLEX III Bruker Daltonics spectrometer using DCTB+ as matrix. High resolution mass spectrometry (HRMS) was performed with a JEOL JMS-700 B/E. Cyclic voltammetry was performed using a Biologic SP-150 potentiostat with positive feedback compensation in 0.10 M Bu₄NPF₆/CH₂Cl₂ (HPLC grade). Experiments were carried out in a one-compartment cell equipped with a platinum working electrode (2 mm of diameter) and a platinum wire counter electrode. A silver wire immersed in 0.10 M Bu₄NPF₆/CH₂Cl₂ was used as pseudo-reference electrode and checked against the ferrocene/ferrocenium couple (Fc/Fc⁺) before and after each experiment. The potentials were then expressed vs Fc/Fc⁺. Photoelectron spectroscopy in air (PESA) were carried out on a Riken AC-2 photoelectron spectrometer (Riken Keiki, Tokyo, Japan).

Absorption spectra were recorded on a JASCO V-650 spectrophotometer in diluted solution (ca. 10⁻⁵ or 10⁻⁶ mol L⁻¹), using spectrophotometric grade solvents. Emission spectra were measured using Horiba-Jobin–Yvon Fluorolog-3 fluorimeter. The steady-state luminescence was excited by unpolarised light from a 450 W xenon continuous wave (CW) lamp and detected at an angle of 90° for measurements of dilute solutions (10 mm quartz cuvette) by using a Hamamatsu R928. Spectra were corrected for both excitation source light-intensity variation and emission spectral responses. Luminescence quantum yields ϕ_f were measured in diluted solutions with an absorbance lower than 0.1, by using the following Equation 1:

$$\phi_{fx}/\phi_{fr} = [A_r(\lambda)/A_x(\lambda)][n_x^2/n_r^2][D_x/D_r] \quad (1)$$

where $A(\lambda)$ is the absorbance (or optical density) at the excitation wavelength, n the refractive index of the solvent and D the integrated luminescence intensity. “r” and “x” stand for reference and sample, respectively. Here, the reference is coumarin-153 in methanol ($\phi_{fr} = 0.45$). Excitations of reference and sample compounds were performed at the same wavelength. The reported results are the average of 4–5 independent measurements at various absorbances (comprised between 0.01–0.1) for both sample and reference. The plot of the integrated luminescence intensity vs. absorbance gives straight line with excellent correlation coefficients and the slope S can be determined for both sample (x) and reference (r).

For singlet oxygen quantum yield determination ϕ_{Δ} , the principle is exactly the same except that the singlet oxygen luminescence emission band (D) is integrated for both sample (x) and reference (r) compounds. $A(\lambda)$ is the absorbance (or optical density) at the excitation wavelength. In this case it is very important that both experiments are conducted in the same

solvent at exactly the same excitation wavelength ($n_x = n_r$). Equation 1 then becomes equation 2

$$\varphi_{\Delta x}/\varphi_{\Delta r} = [A_r(\lambda)/A_x(\lambda)][n_x^2/n_r^2][D_x/D_r] \quad (2=)$$

The reported results are the average of 4–5 independent measurements at various absorbances (comprised between 0.01–0.1) for both sample and reference. The plot of the integrated singlet oxygen luminescence intensity vs. absorbance gives straight line with excellent correlation coefficients and the slope S can be determined for both sample (x) and reference (r). In the present case, the reference is phenalenone ($\varphi_{\Delta r} = 0.98$ in dichloromethane).

Excited state lifetime analyses were measured at the maximum emission wavelength using a 440nm nanoLED by means of the time correlated single photon counting (TCSPC) method of diluted dichloromethane solutions at room temperature.

Synthetic procedures

5-bromo-11-nitro-2-(pentan-3-yl)-1H-thioxantheno[2,1,9-def]isoquinoline-1,3(2H)-dione

(NO₂-BTI-Br): HNO₃ (0.19 mL, 4.42 mmol) was added over a stirred solution of **BTI-Br** (1.00 g, 2.21 mmol) in CH₂Cl₂ (120 mL) under air. After 20 minutes, the reaction was quenched with water and the organic phase was extracted with CH₂Cl₂, dried with MgSO₄ and concentrated under reduced pressure. The crude was purified by column chromatography on silica gel (eluent: CH₂Cl₂) yielding **NO₂-BTI-Br** (0.99 g, 90%) as a red powder. ¹H NMR (300 MHz, CDCl₃): δ (ppm) 8.89 (s, 1H), 8.76 (s, 1H), 7.71 – 7.62 (m, 2H), 7.55 (td, $J = 7.6, 1.2$ Hz, 1H), 7.43 (ddd, $J = 8.5, 7.2, 1.3$ Hz, 1H), 5.09 – 4.89 (m, 1H), 2.33 – 2.11 (m, 2H), 2.02 – 1.82 (m, 2H), 0.88 (t, $J = 7.5$ Hz, 6H). ¹³C NMR (75 MHz, CDCl₃): δ (ppm) 146.4, 141.0, 136.1, 133.5, 131.4, 129.7, 129.4, 129.2, 128.7, 128.7, 128.4, 127.6, 125.4, 124.6, 116.7, 58.1, 24.9, 11.4. **HRMS** (FAB): m/z calcd for C₂₃H₁₇BrN₂O₄S: 496.0087, found: 496.0083. Monocrystals were obtained by slow evaporation of toluene.

5-bromo-2-(pentan-3-yl)indolo[4',3',2':3,4,5]isothiochromeno[7,8,1-def]isoquinoline-

1,3(2H,10H)-dione (NH-TCI-Br): **NO₂-BTI-Br** (115.0 mg, 0.23 mmol) and triphenylphosphine (194.1 mg, 0.74 mmol) were dissolved in DMF (3.2 mL) under argon. The mixture was refluxed for 40 h and then the solvent was removed in vacuo and the resulting crude was filtered through a plug of neutral alumina washing thoroughly with chloroform. After removing the solvent, the crude was slurried in CH₂Cl₂ and filtered to obtain compound **NH-TCI-Br** (75 mg, 70%) as a reddish powder. ¹H NMR (300 MHz, DMSO-*d*₆): δ (ppm) 11.87 (s, 1H), 8.51 (s, 1H), 8.14 (s, 1H), 7.46 (t, $J = 8.2$ Hz, 1H), 7.34 (d, $J = 8.1$ Hz, 1H), 7.20 – 7.11 (m, 1H), 5.06 – 4.91 (m, 1H), 2.28 – 2.07 (m, 2H), 1.94 – 1.78 (m, 2H), 0.83 (t, $J = 7.4$ Hz, 6H). **HRMS** (FAB): m/z calcd for C₂₃H₁₇BrN₂O₂S: 464.0189, found: 464.0159. The product was not soluble enough to obtain a ¹³C NMR spectrum.

5-bromo-10-hexyl-2-(pentan-3-yl)indolo[4',3',2':3,4,5]isothiochromeno[7,8,1-

def]isoquinoline-1,3(2H,10H)-dione (TCI-Br): Compound **13** (60.0 mg, 0.13 mmol) and K₂CO₃ (34.8 mg, 0.25 mmol) were dissolved in DMF (3 mL) and then 1-bromohexane (33 μ L, 0.24 mmol) was added. The mixture was heated at 120 °C for 16 h. Water was added to quench the reaction and the precipitate was filtered off and washed with water and methanol yielding **TCI-Br** (53 mg,

75%) as an orange powder. ¹H NMR (300 MHz, CDCl₃): δ (ppm) 8.56 (s, 1H), 8.33 (s, 1H), 7.40 (dd, *J* = 8.2, 7.5 Hz, 1H), 7.11 (d, *J* = 8.2 Hz, 1H), 7.02 (d, *J* = 7.5 Hz, 1H), 5.11 – 4.97 (m, 1H), 4.31 (t, *J* = 7.2 Hz, 2H), 2.28 – 2.11 (m, 2H), 1.95 – 1.77 (m, 4H), 1.36 – 1.15 (m, 6H), 0.90 – 0.73 (m, 9H). ¹³C NMR (75 MHz, CDCl₃): δ (ppm) 141.5, 140.9, 134.2, 132.5, 130.2, 129.8, 123.1, 121.9, 121.9, 118.9, 114.0, 113.9, 107.4, 57.7, 45.1, 31.6, 29.9, 26.9, 25.2, 22.6, 14.1, 11.5. HRMS (FAB): *m/z* calcd for C₂₉H₂₉BrN₂O₂S: 548.1128, found: 548.1116.

10-hexyl-2-(pentan-3-yl)indolo[4',3',2':3,4,5]isothiochromeno[7,8,1-def]isoquinoline-1,3(2H,10H)-dione (TCI): TCI-Br (60.0 mg, 0.11 mmol), sodium *tert*-butoxyde (11.0 mg, 0.11 mmol) and (NHC)Pd(allyl)Cl (1.9 mg, 3.3 μmol) were dissolved in isopropyl alcohol (3 mL) and stirred at 60 °C for 2 hours. Then the solvent was removed in vacuo and the product was purified by column chromatography on silica gel (eluent: CH₂Cl₂) yielding TCI (44.0 mg, 86%) as an orange powder. ¹H NMR (300 MHz, CDCl₃): δ (ppm) 8.50 (s, 1H), 8.18 (d, *J* = 8.0 Hz, 1H), 7.39 – 7.30 (m, 2H), 7.01 (d, *J* = 8.2 Hz, 1H), 6.89 (d, *J* = 7.5 Hz, 1H), 5.23 – 5.05 (m, 1H), 4.24 (t, *J* = 7.2 Hz, 2H), 2.40 – 2.20 (m, 2H), 2.04 – 1.80 (m, 4H), 1.41 – 1.21 (m, 6H), 0.94 (t, *J* = 7.5 Hz, 6H), 0.85 (t, *J* = 7.0 Hz, 3H). ¹³C NMR (75 MHz, CDCl₃): δ (ppm) 165.3, 141.5, 140.9, 133.7, 130.1, 129.5, 129.0, 123.5, 122.1, 121.4, 120.3, 119.4, 118.8, 116.2, 113.5, 107.0, 57.5, 44.8, 31.6, 29.9, 26.9, 25.2, 22.6, 14.1, 11.6. HRMS (EI): *m/z* calcd for C₂₉H₃₀N₂O₂S: 470.2022, found: 470.2031. Monocrystals were obtained by slow evaporation of toluene.

11,11'-dinitro-2,2'-di(pentan-3-yl)-1H,1'H-[5,5'-bithioxantheno[2,1,9-def]isoquinoline]-1,1',3,3'(2H,2'H)-tetraone (BTI₂-NO₂): HNO₃ (51 μL, 1.21 mmol) was added under air over a stirred solution of BTI₂ (225.0 mg, 0.30 mmol) in CH₂Cl₂ (15 mL). After 20 minutes, the reaction was quenched with water and the organic phase was extracted with CH₂Cl₂, dried with MgSO₄ and concentrated under reduced pressure yielding BTI₂-NO₂ (252 mg, 100%) as a reddish powder. ¹H NMR (300 MHz, CDCl₃): δ (ppm) 8.99 (s, 1H), 8.50 (s, 1H), 7.70 (d, *J* = 7.1 Hz, 1H), 7.48 – 7.33 (m, 3H), 5.13 – 5.00 (m, 1H), 2.34 – 2.16 (m, 2H), 2.03 – 1.86 (m, 2H), 0.93 (t, *J* = 7.3 Hz, 6H). ¹³C NMR (75 MHz, CDCl₃): δ (ppm) 146.5, 140.6, 133.8, 133.2, 131.9, 131.3, 131.0, 130.6, 129.8, 128.7, 128.5, 127.5, 124.8, 122.4, 119.5, 58.3, 25.0, 11.5. HRMS (MALDI): *m/z* calcd for C₄₆H₃₄N₄O₈S₂: 834.1813, found: 834.1825.

10,10'-dihexyl-2,2'-di(pentan-3-yl)-[5,5'-biindolo[4',3',2':3,4,5]isothiochromeno[7,8,1-def]isoquinoline]-1,1',3,3'(2H,2'H,10H,10'H)-tetraone (TCI₂): 11,11'-dinitro-2,2'-di(pentan-3-yl)-1H,1'H-[5,5'-bithioxantheno[2,1,9-def]isoquinoline]-1,1',3,3'(2H,2'H)-tetraone (277.0 mg, 0.33 mmol) and triphenylphosphine (556.9 mg, 2.1 mmol) were dissolved in DMF (7 mL) under argon. The mixture was refluxed for 40 h and then the solvent was removed in vacuo. The resulting crude was slurried in petroleum ether and washed with petroleum ether and washed with an 8:2 petroleum ether/CH₂Cl₂ mixture. The resulting crude was dissolved in DMF (9 mL) along with K₂CO₃ (132.6 mg, 0.96 mmol) and then 1-bromohexane (0.27 mL, 1.92 mmol) was added. The mixture was heated at 120 °C for 16 h. Water was added to quench the reaction and the precipitate was filtered off and washed with water and methanol. Then, after removing the solvent in vacuo, the crude was filtered through a plug of silica washing thoroughly with CH₂Cl₂ yielding TCI₂ (135 mg, 56%) as an orange powder. ¹H NMR (300 MHz, CDCl₃): δ (ppm) 8.73 (s, 1H), 8.32 (s, 1H), 7.39 (t, *J* = 7.9 Hz, 1H), 7.17 (d, *J* = 8.2 Hz, 1H), 6.90 (d, *J* = 7.5 Hz, 1H), 5.23 – 5.10 (m, 1H), 4.43 (t, *J* = 7.1 Hz, 2H), 2.39 – 2.23 (m, 2H), 2.04 – 1.88 (m, 4H), 1.46 – 1.23 (m, 6H),

1.02 – 0.82 (m, 9H). ^{13}C NMR (75 MHz, CDCl_3): δ (ppm) 165.3, 140.9, 134.0, 130.4, 130.1, 129.6, 123.2, 122.4, 122.1, 119.6, 118.8, 113.7, 107.1, 57.5, 44.9, 31.5, 29.8, 26.9, 25.2, 22.6, 14.1, 11.6. HRMS (MALDI): m/z calcd for $\text{C}_{58}\text{H}_{58}\text{N}_4\text{O}_4\text{S}_2$: 938.3894, found: 938.3896.

NMR spectra

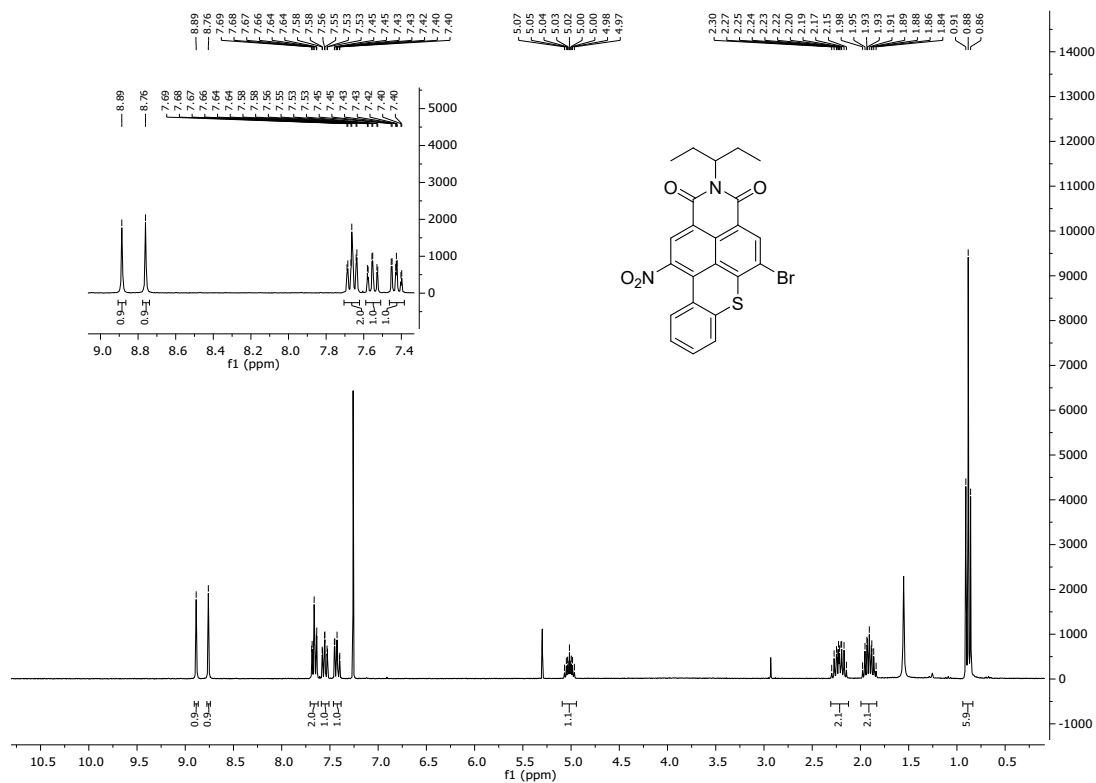


Figure S1. ^1H NMR (CDCl_3 , 300 MHz) spectrum of $\text{NO}_2\text{-BTI-Br}$.

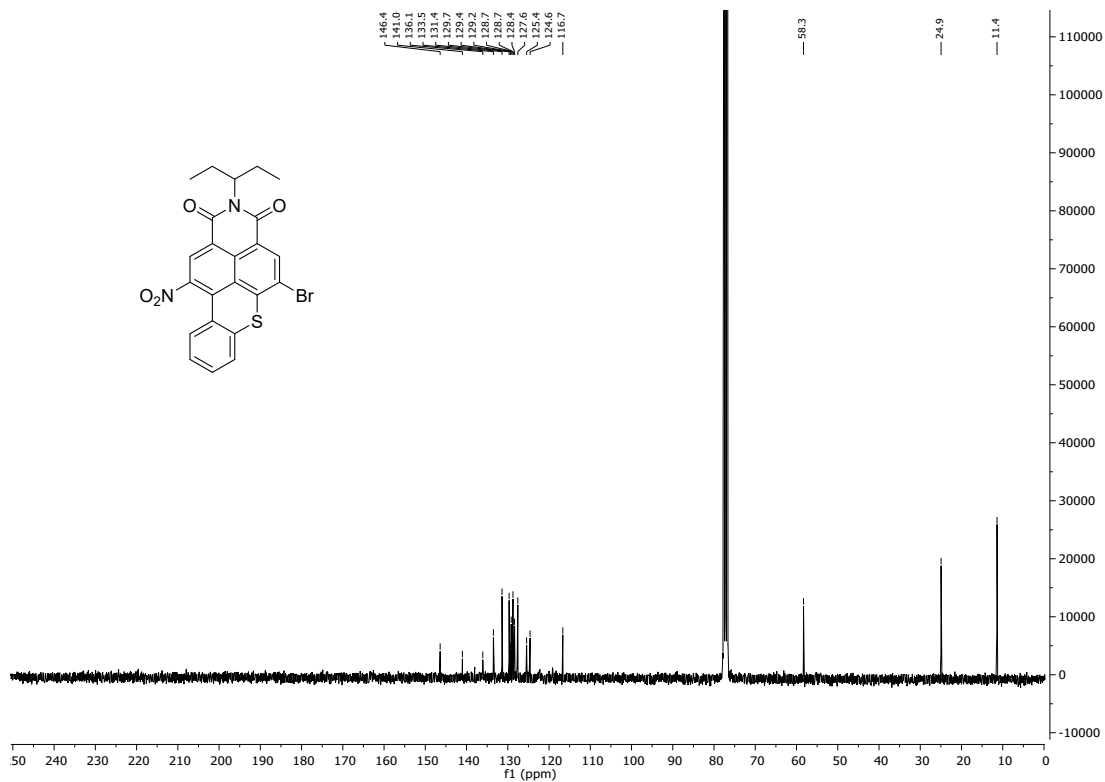


Figure S2. ¹³C NMR (CDCl₃, 75 MHz) spectrum of **NO₂-BTI-Br**.

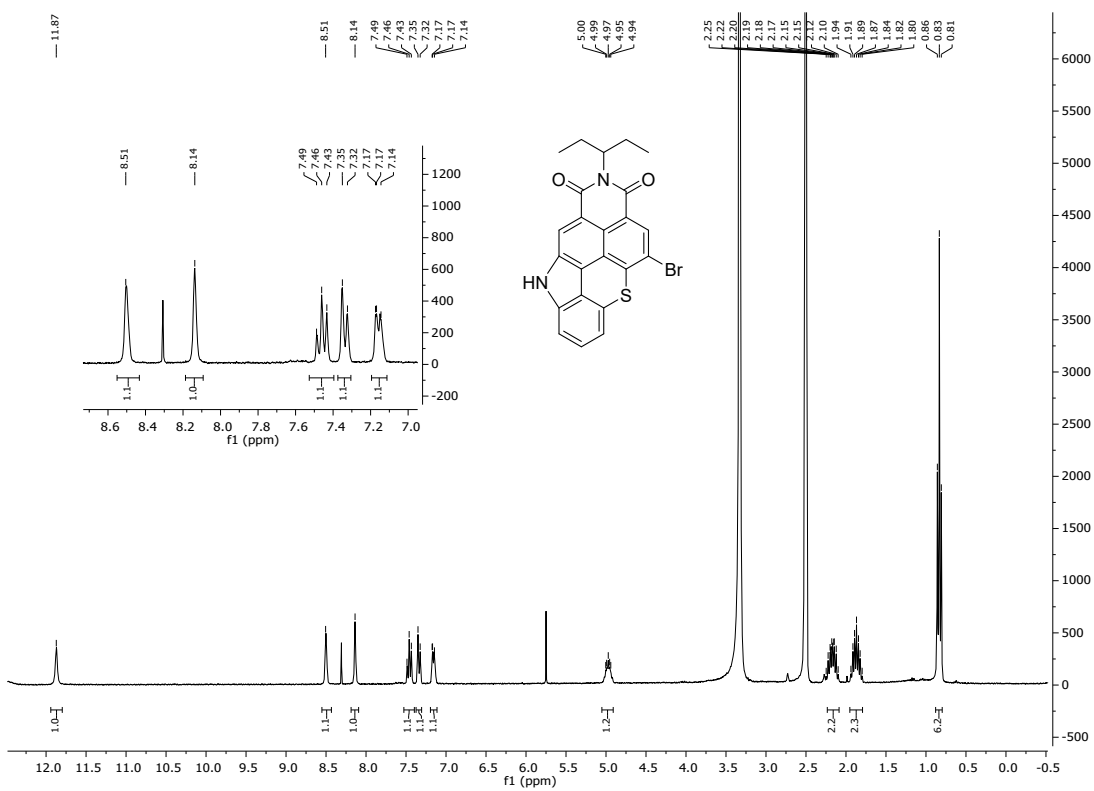


Figure S3. ¹H NMR (DMSO-*d*₆, 300 MHz) spectrum of **NH-TCI-Br**.

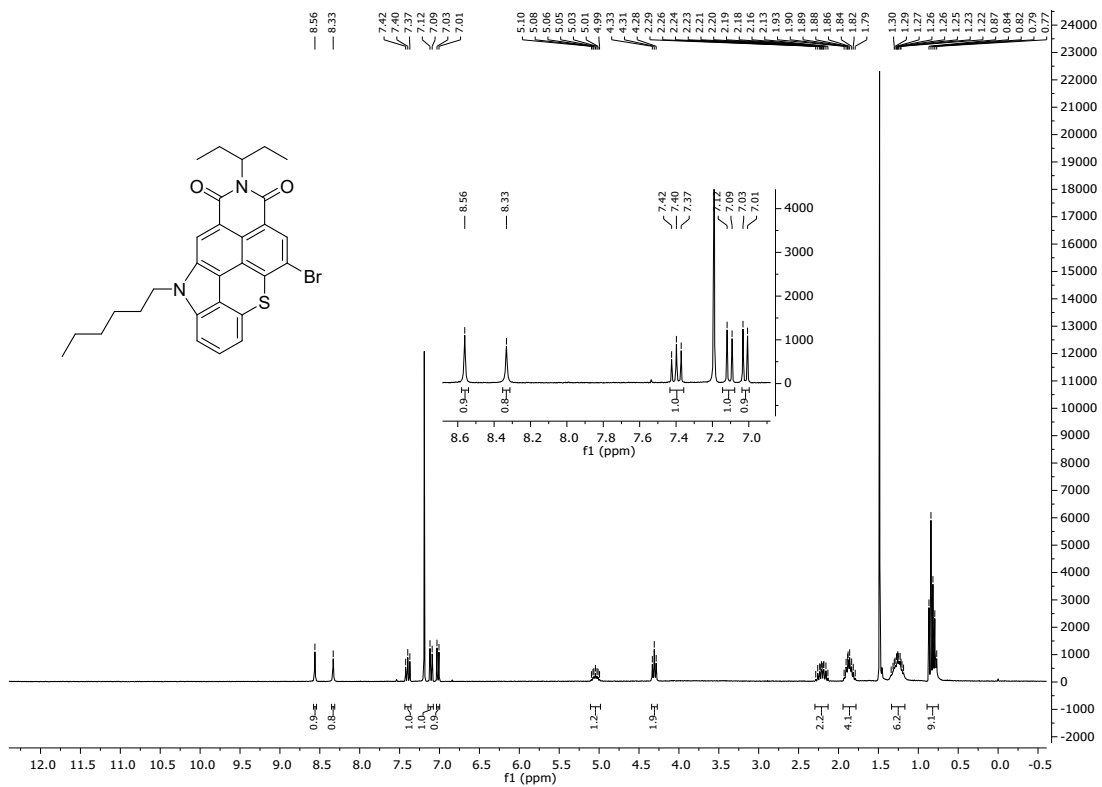


Figure S4. ^1H NMR (CDCl_3 , 300 MHz) spectrum of TCI-Br.

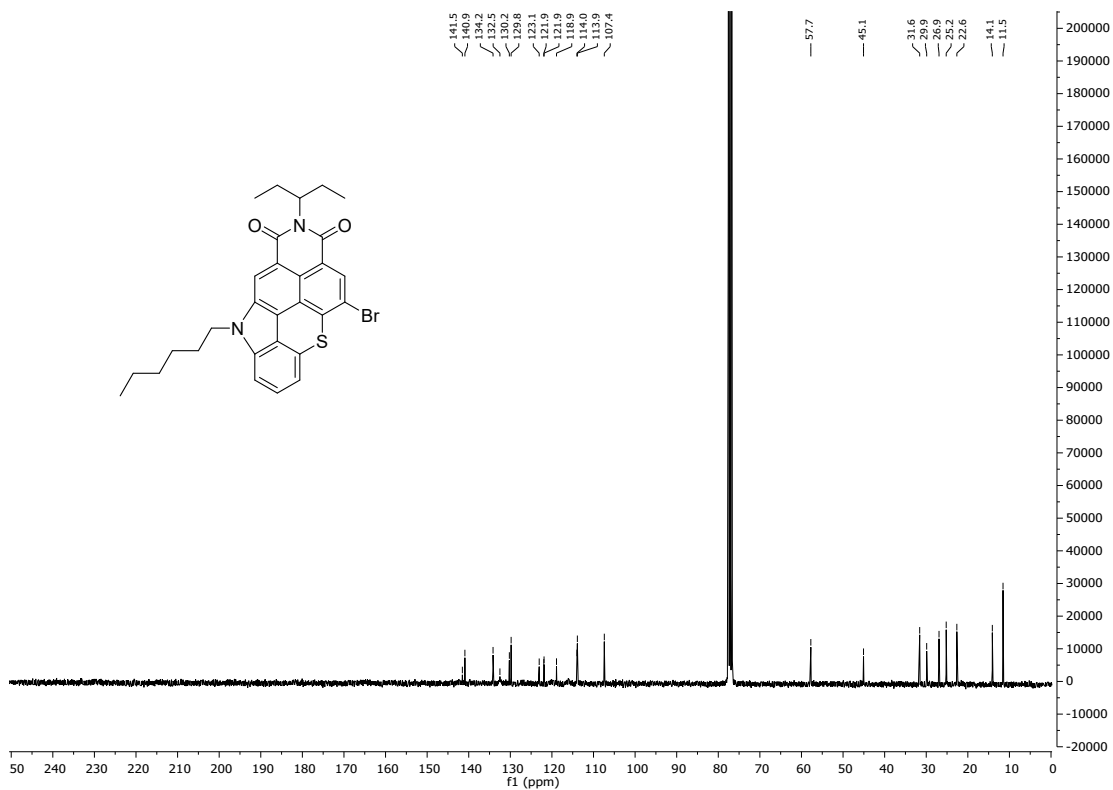


Figure S5. ^{13}C NMR (CDCl_3 , 75 MHz) spectrum of TCI-Br.

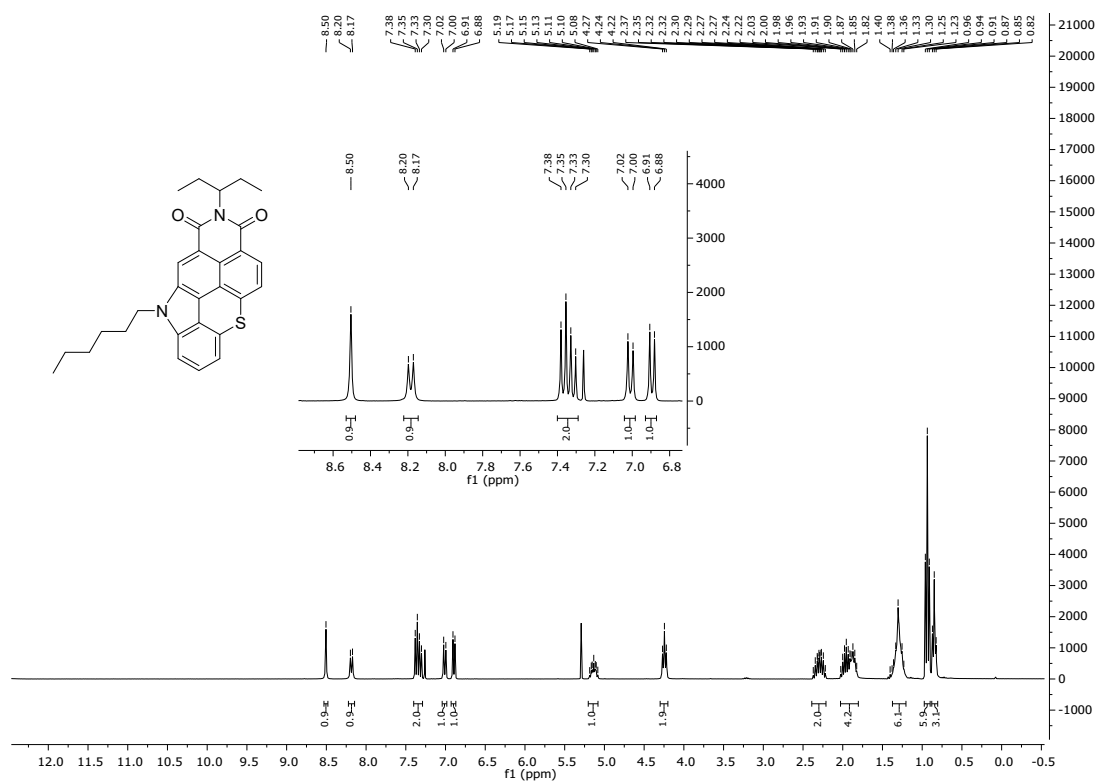


Figure S6. ^1H NMR (CDCl_3 , 300 MHz) spectrum of TCI.

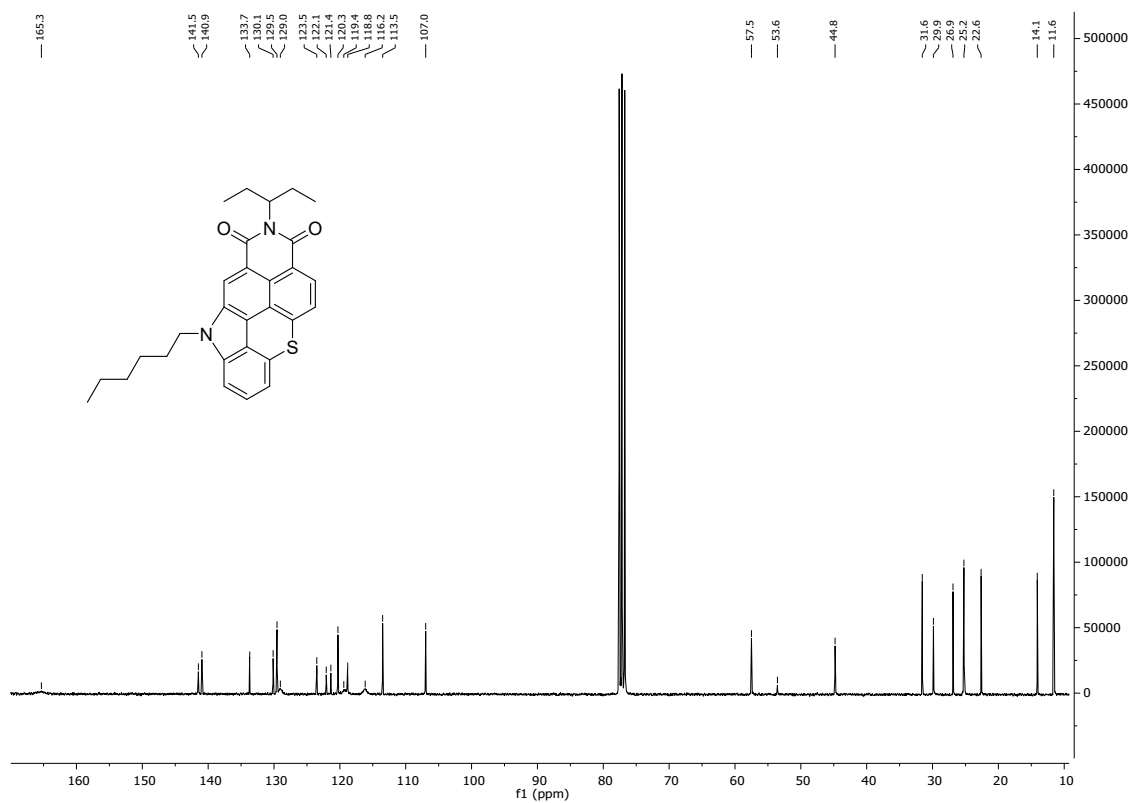


Figure S7. ^{13}C NMR (CDCl_3 , 75 MHz) spectrum of TCI.

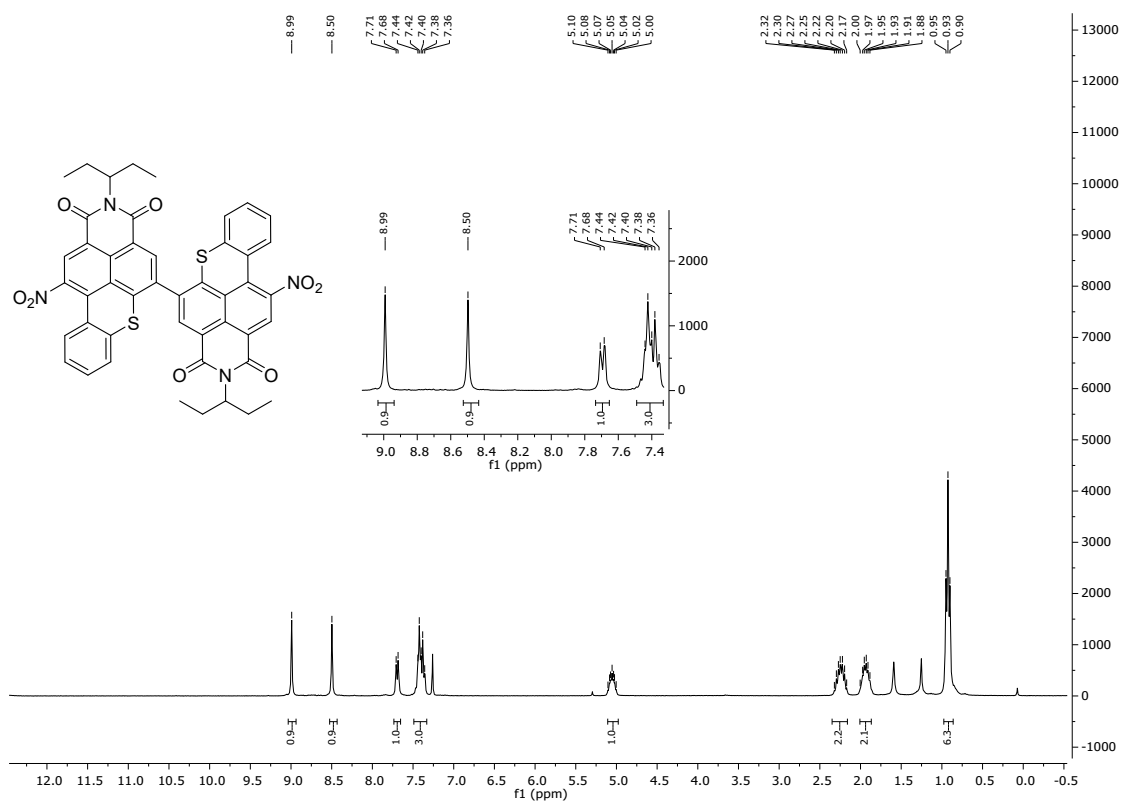


Figure S8. ¹H NMR (300 MHz, CDCl₃) spectrum of BTI₂-NO₂.

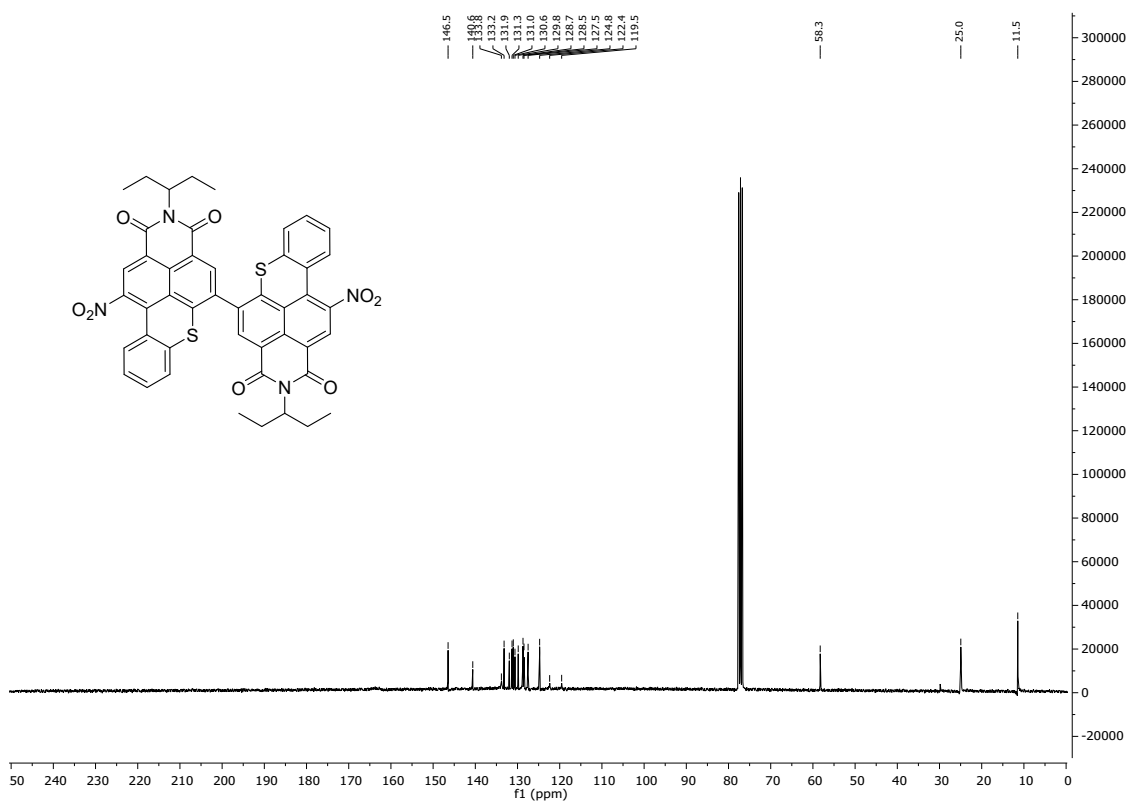


Figure S9. ¹³C NMR (75 MHz, CDCl₃) spectrum of BTI₂-NO₂.

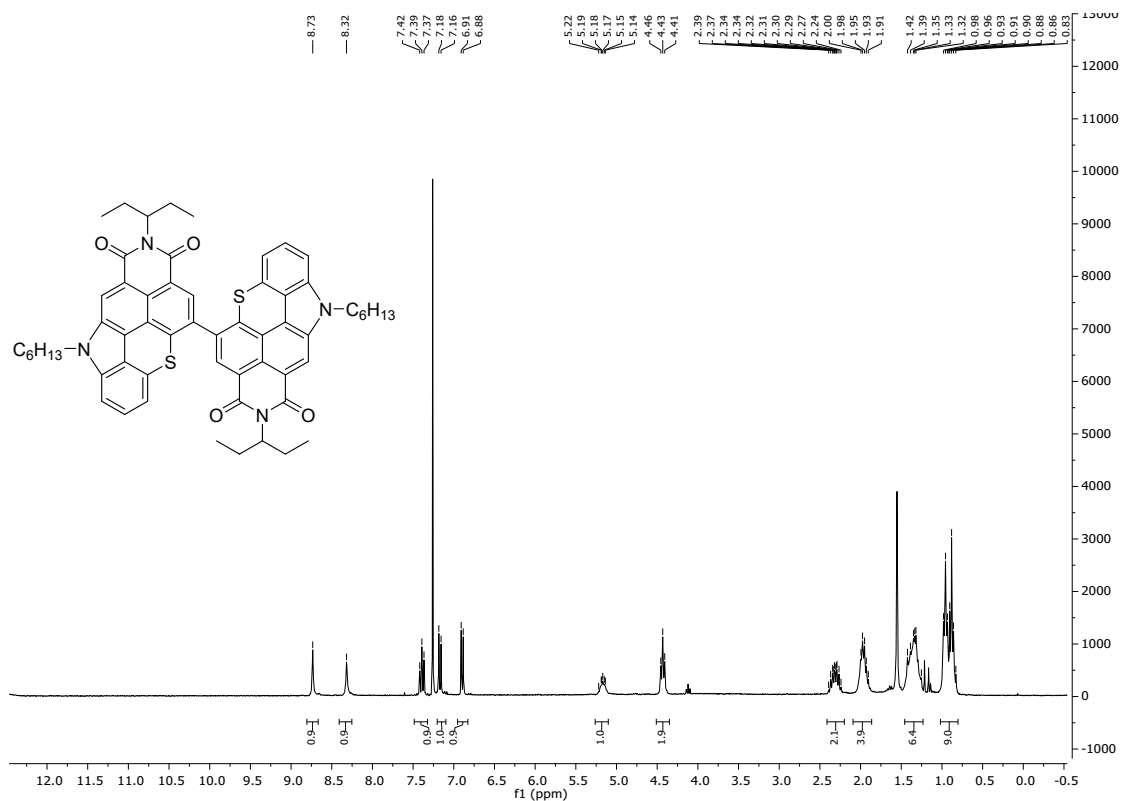


Figure S10. ¹H NMR (300 MHz, CDCl₃) spectrum of TCl₂.

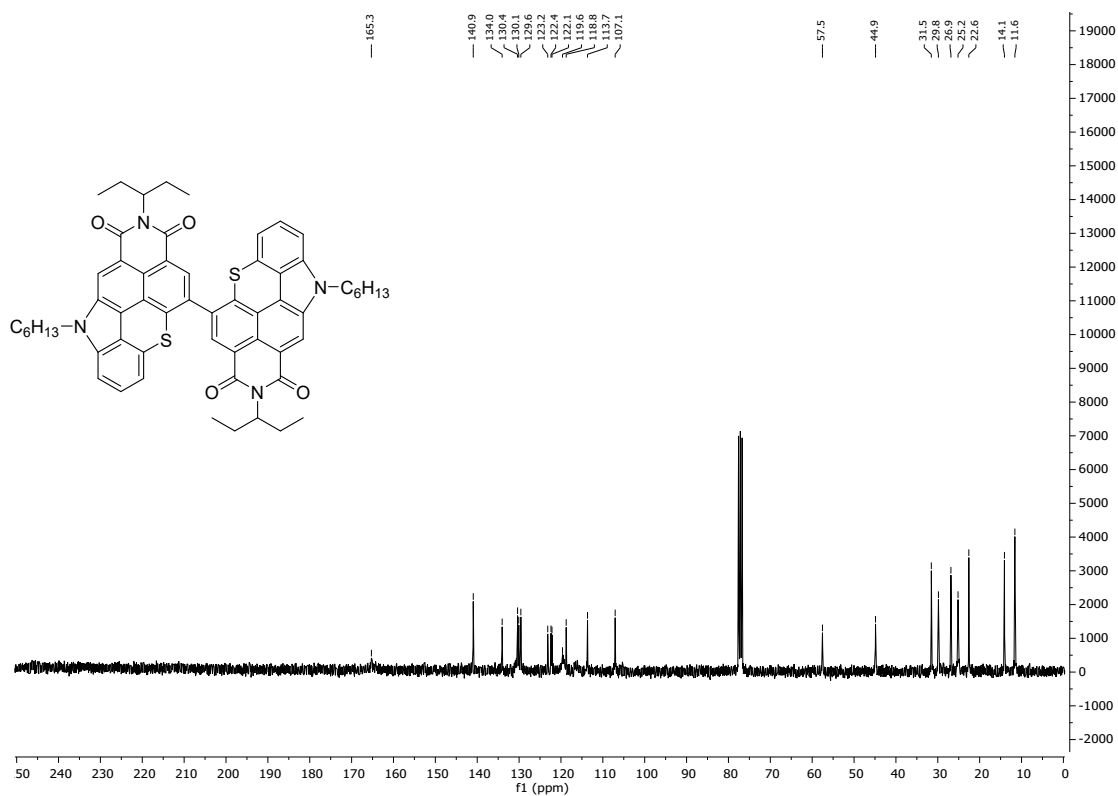
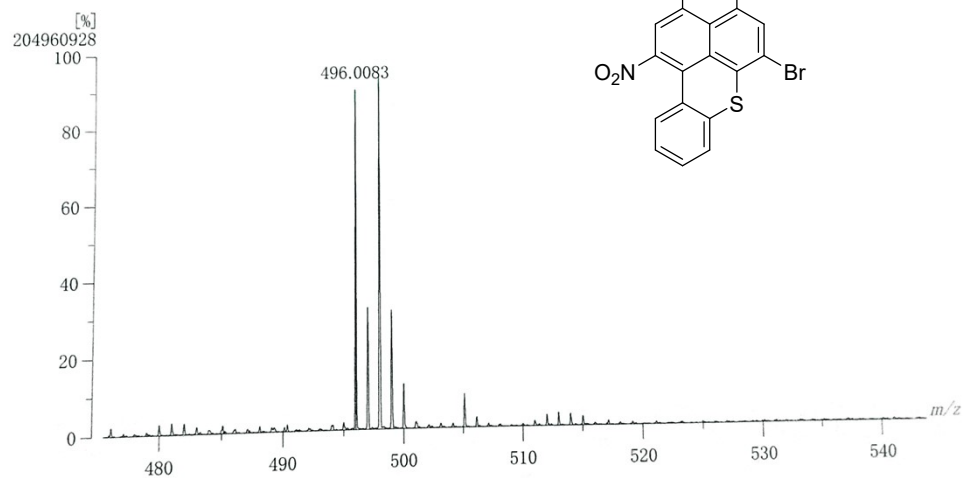


Figure S11. ¹³C NMR (75 MHz, CDCl₃) spectrum of TCl₂.

HRMS Spectra

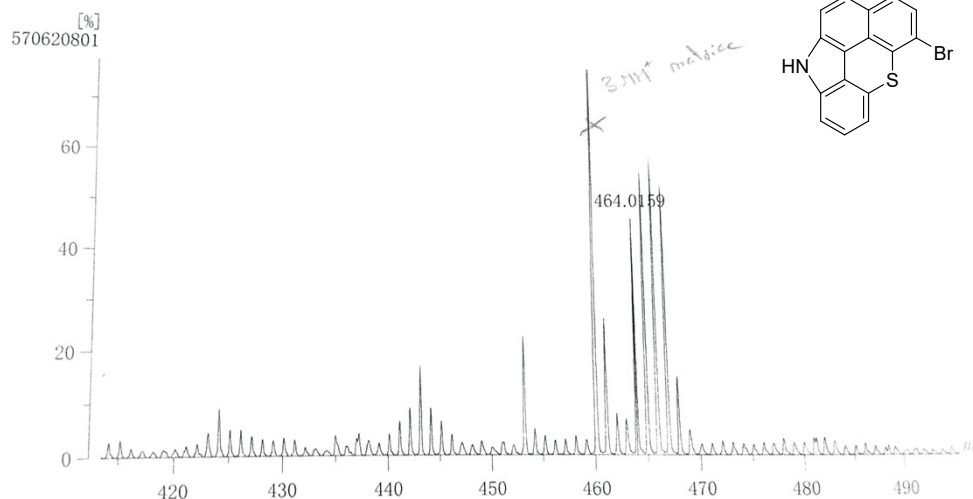
[Mass Spectrum]
 Data : JMA252-FAB-Xe-neg001 Date : 06-May-2019 09:45
 RT : 3.96 min Scan# : (506,554)
 Elements : C 24/0, H 49/0, Br 1/0, N 2/0, O 4/0, S 1/0
 Mass Tolerance : 1000ppm, 1mmu if m/z > 1
 Unsaturation (U.S.) : -0.5 - 30.0



Observed m/z	Int%	Err [ppm / mmu]	U.S. Composition
1 496.0083	90.51	-1.9 / -0.9	17.0 C23 H17 Br N2 O4 S

Figure S12. HRMS (FAB) spectrum of **NO₂-BTI-Br**: *m/z* calcd for C₂₃H₁₇BrN₂O₄S: 496.0087, found: 496.0083.

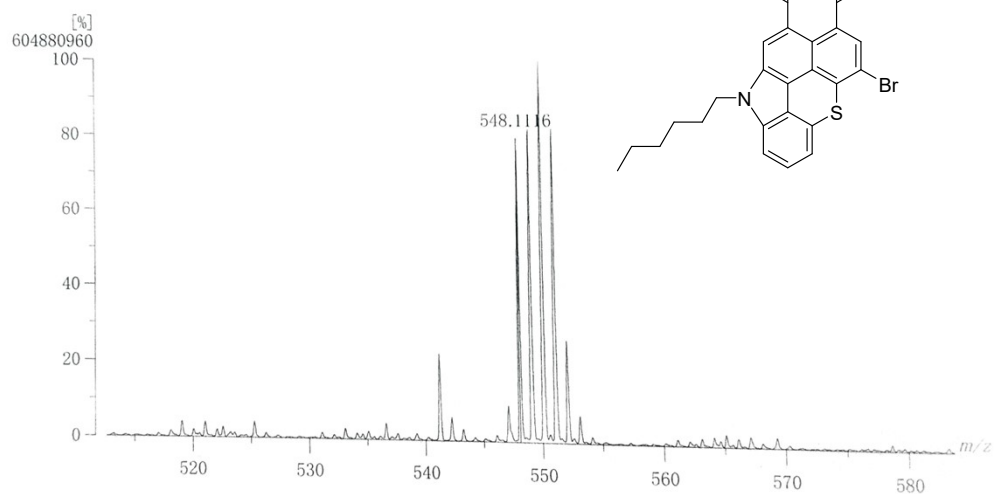
[Mass Spectrum]
 Data : JMA257-FABposXe001 Date : 28-Jun-2019 10:06
 RT : 0.56 min Scan# : (113,198)
 Elements : C 24/0, H 49/0, Br 1/0, N 2/0, O 2/0, S 2/0
 Mass Tolerance : 1000ppm, 2mmu if m/z > 2
 Unsaturation (U.S.) : -0.5 - 20.0



Observed m/z	Int%	Err [ppm / mmu]	U.S. Composition
1 464.0159	46.78	+3.6 / +1.7	17.5 C24 H19 Br N S2

Figure S13. HRMS (FAB) spectrum of **NH-TCI-Br**: *m/z* calcd for C₂₃H₁₇BrN₂O₂S: 464.0189, found: 464.0159.

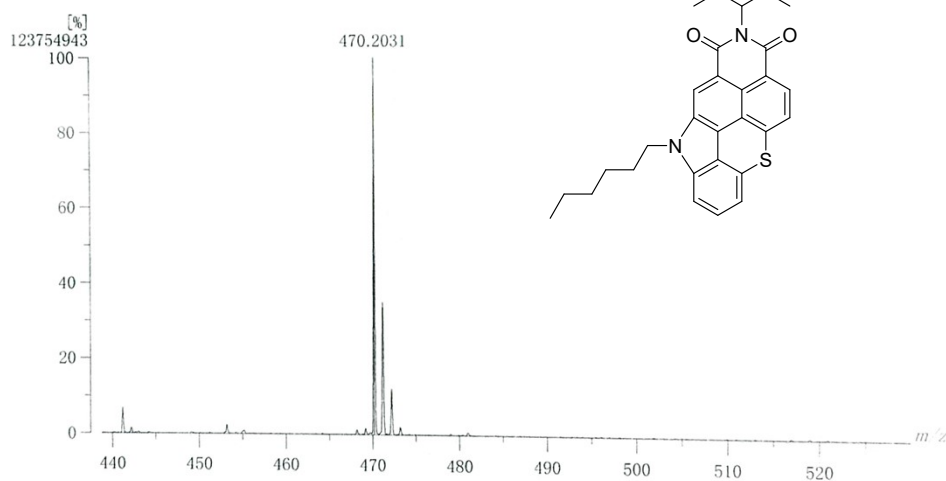
[Mass Spectrum]
 Data : JMA259-FABposXe001 Date : 28-Jun-2019 10:13
 RT : 3.64 min Scan# : (824,919)
 Elements : C 30/0, H 49/0, Br 1/0, N 2/0, O 2/0, S 2/0
 Mass Tolerance : 1000ppm, 2mmu if m/z > 2
 Unsaturation (U.S.) : -0.5 - 30.0



Observed m/z	Int%	Err [ppm / mmu]	U.S. Composition
1 548.1116	79.63	-3.1 / -1.7	17.0 C29 H29 Br N2 O2 S

Figure S14. HRMS (FAB) spectrum of **TCI-Br**: m/z calcd for $C_{29}H_{29}BrN_2O_2S$: 548.1128, found: 548.1116

[Mass Spectrum]
 Data : JMA272-EI001 Date : 03-Sep-2019 16:01
 RT : 16.39 min Scan# : (3725,3916)
 Elements : C 30/0, H 49/0, N 2/0, O 2/0, S 1/0
 Mass Tolerance : 1000ppm, 1mmu if m/z > 1
 Unsaturation (U.S.) : -0.5 - 30.0



Observed m/z	Int%	Err [ppm / mmu]	U.S. Composition
1 470.2031	100.00	+0.6 / +0.3	17.0 C29 H30 N2 O2 S

Figure S15. HRMS (EI) spectrum of **TCI**: m/z calcd for $C_{29}H_{30}N_2O_2S$: 470.2022, found: 470.2031.

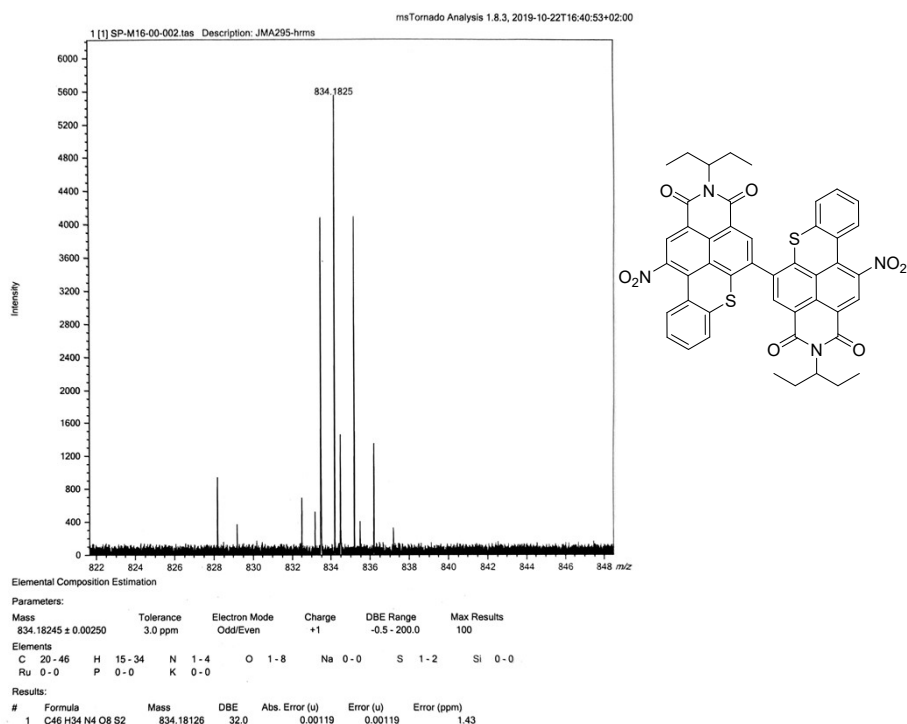


Figure S16. HRMS (MALDI) spectrum of **BTI₂-NO₂**: m/z calcd for C₄₆H₃₄N₄O₈S₂: 834.1813, found: 834.1825

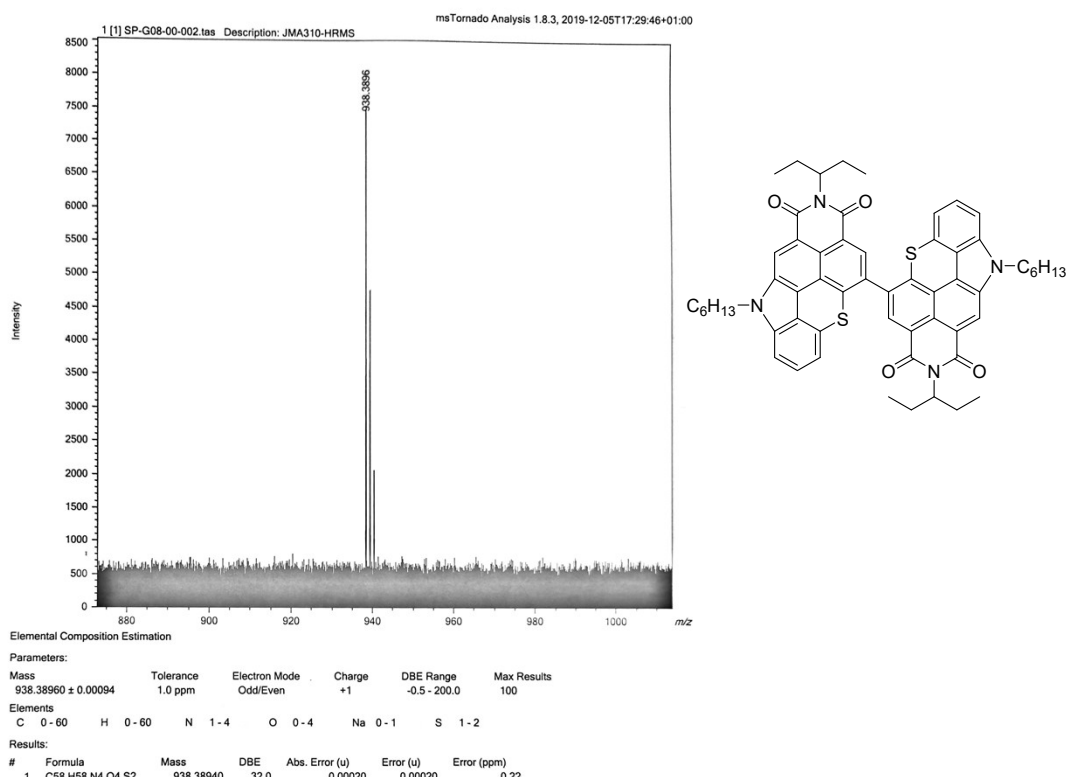


Figure S17. HRMS (MALDI) spectrum of **TCI₂**: m/z calcd for C₅₈H₅₈N₄O₄S₂: 938.3894, found: 938.3896

Crystallographic data

Table S1. Crystal data collection and refinement parameters of **NO₂-BTI-Br**, **BTI** and **TCI**.

Molecule	NO₂-BTI-Br	BTI	TCI
Empirical formula	C ₂₃ H ₁₇ BrN ₂ O ₄ S, C ₇ H ₈	C ₂₃ H ₁₉ NO ₂ S	C ₂₉ H ₃₀ N ₂ O ₂ S
Formula weight	589.49	373.45	470.61
Temperature (K)	150.0(1)	150.0(1)	200.0(1)
Crystal system, space group	Monoclinic, <i>P</i> 2 ₁ / <i>c</i>	Triclinic, <i>P</i> -1	Triclinic, <i>P</i> -1
<i>a</i> (Å)	17.2992(3)	7.4198(5)	7.9966(3)
<i>b</i> (Å)	7.1337(1)	8.8854(5)	11.5642(5)
<i>c</i> (Å)	22.0936(4)	15.1195(9)	12.9910(5)
α (deg)	90	101.609(5)	84.758(3)
β (deg)	109.488(2)	90.283(5)	87.196(3)
γ (deg)	90	111.324(5)	86.447(3)
Volume (Å ³)	2570.31(8)	906.22(10)	1192.88(8)
<i>Z</i>	4	2	2
Calculated density (Mg/m ³)	1.523	1.369	1.310
Absorption coefficient (mm ⁻¹)	3.275	1.728	1.434
θ range (deg)	2.709 to 72.003	5.476 to 76.310	3.420 to 76.252
Data collected / unique [<i>R</i> _{int}]	11136 / 4949 [0.0254]	6684 / 3620 [0.0329]	9313 / 4772 [0.0176]
<i>R</i> ₁ / <i>wR</i> ₂ [<i>I</i> > 2 σ (<i>I</i>)]	0.0421 / 0.1130	0.0644 / 0.1867	0.0771 / 0.2297
<i>R</i> ₁ / <i>wR</i> ₂ [all data]	0.0437 / 0.1147	0.0681 / 0.1955	0.0842 / 0.2413
GOF	1.042	1.032	1.062
Largest diff. peak & hole (e/Å ³)	1.481 & -0.702	0.551 and - 0.300	1.175 & -0.637
CCDC number	2083064	2083265	2083068

X-ray single-crystal diffraction data were collected on a Rigaku Oxford Diffraction SuperNova diffractometer equipped with Atlas CCD detector and micro-focus Cu-K α radiation (1.54184 Å). The structures were solved by by dual-space algorithm and refined on *F*² by full matrix least-squares techniques using SHELX programs (G. M. Sheldrick, SHELXT and SHELXL 2014-2018). All non-H atoms were refined anisotropically and multiscan empirical absorption was corrected using CrysAlisPro program (CrysAlisPro, Agilent Technologies, V 1.171.40.45a, 2019). The H atoms were included in the calculation without refinement.

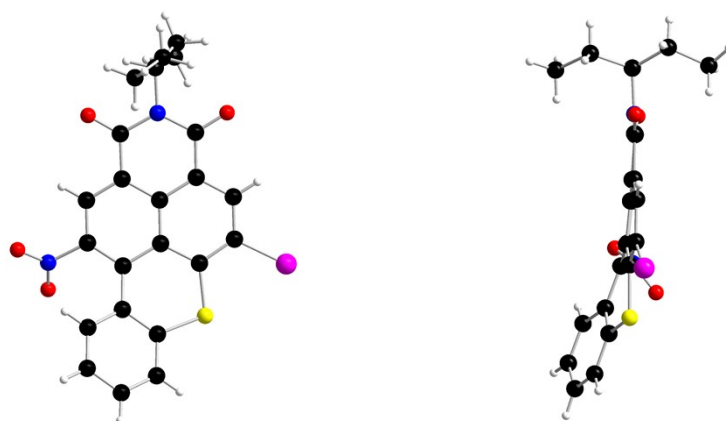


Figure S18. Molecular structure of **NO₂-BTI-Br** obtained by X-ray crystallography.

The planar BT cores of BTI molecules overlap and stack along the *a* axis in a head-to-tail manner with distances between the BT cores comprises between 3.477 Å and 3.569 Å. The planar BT core of TCI molecules overlap as dimers in a head to tail manner with hexyl chains in opposite direction and with a distance of 3.471 Å. The next dimer alternates as a stair, with a small shift due to hexyl chains, at a distance of 3.547 Å.

Optical data .

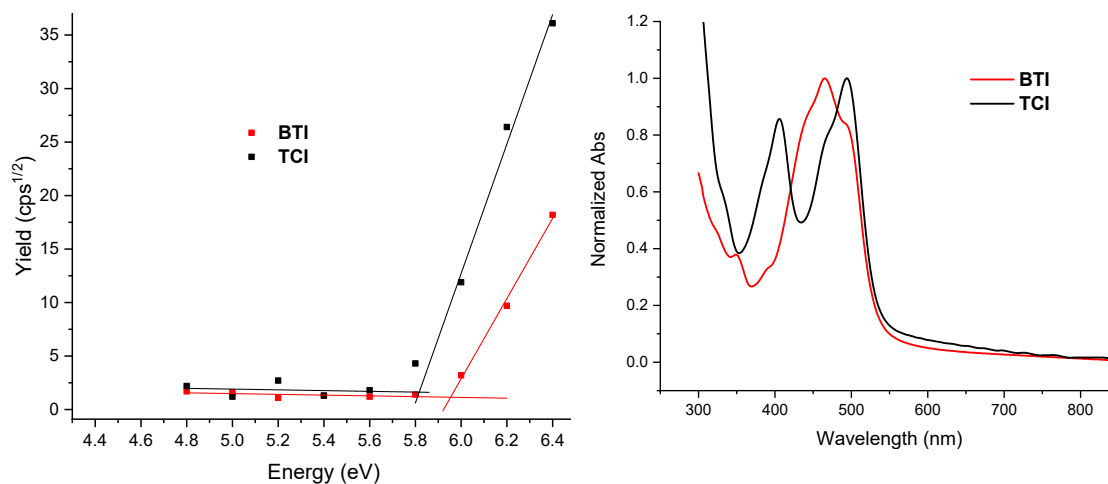


Figure S19. Photoemission spectra (left) and UV-Vis spectra on glass (right) of **BTI** and **TCI**.

Table S2. Estimated energy levels of **BTI** and **TCI** as spun casted films.

Molecule	HOMO (eV) ^a	E _g ^{opt} (eV) ^b	LUMO (eV) ^c
BTI	-6.01	2.31	3.70
TCI	-5.82	2.30	-3.52

^a HOMO energy in solid state determined by PESA. ^b Optical gap estimated through the low-energy absorption onset. ^c Obtained through the equation: LUMO = HOMO + E_g^{opt}.

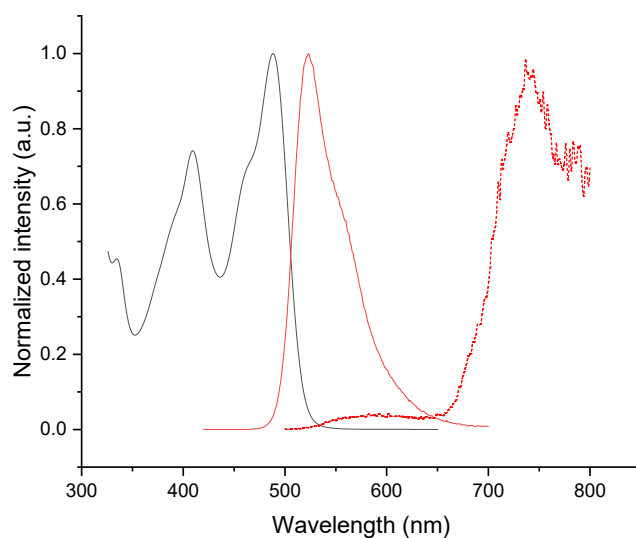


Figure S20 Absorption (black, full) and fluorescence (red, full) spectra of TCl_2 at 298K. Phosphorescence of TCl_2 (red, dashed) at 77K, using 0.1 ms delay

Computed data

All geometries were optimized with Gaussian16 software,¹ using DFT and TD-DFT with the CAM-B3LYP functional,² the 6-31G(d) basis set, in PCM dichloromethane as solvent and using the empirical dispersion correction D3-BJ.³ For TCl_2 , the geometries were optimized at the S_0 and S_1 states such as performing a relaxed scan of the θ angle from 0° to 180° per 15° steps. Computed vertical electronic transitions (Table S3 and Figure S22) presents a blue-shift compared to experiment, that is the expected behavior of the CAM-B3LYP functional. This functional was chosen to reproduce the excitonic coupling of TCl_2 since this coupling needs an accurate description of the long-range electronic interaction.

The Spin-Orbit Coupling between the S_1 state and the triplet states lower in energy were computed on the geometries optimized for the S_1 state. The SOC was computed using the Douglas-Kroll Hamiltonian along with the spin-orbit mean field approach as implemented in the Dalton16 package.⁴ We used the CAM-B3LYP functional and the cc-pVDZ basis set adapted for the

Douglas-Kroll calculations. The CH_2Cl_2 solvent was included along with a PCM in the IEF-PCM approach.

Table S3. Five first vertical transitions calculated for **BTI**, **TCI** and **TCI₂** (only mono-electronic transitions contributing to more than 10% of the total transition are presented)

Molecule	λ (nm)	Oscillator	Main transition	Minor transition
BTI	407	0.60	H->L	-
	320	0.03	H->L+1 (48%)	H->L+2 (22%), H-2->L (11%), H-1->L(10%)
	299	0.01	H->L+2 (35%)	H-2->L (31%), H->L+1 (25%)
	283	0.14	H-1->L (61%)	H->L+3 (15%), H-1->L+1 (13%)
	275	0.00	H-4->L (49%)	H-4->L+5 (12%), H-6->L+1 (12%)
TCI	392	0.39	H->L	-
	330	0.24	H-1->L (55%)	H->L+2 (17%), H->L+1 (17%), H-1->L(10%)
	309	0.01	H->L+1 (75%)	H-1->L (25%)
	276	0.00	H-4->L (61%)	H-7->L+1 (14%), H-4->L+6 (14%)
	275	0.08	H-2->L (39%)	H-1->L+1 (17%), H->L+2 (17%), H->L+1 (12%)
TCI₂	402	0.50	H->L+1 (51%)	H-1->L (49%)
	401	0.24	H-1->L (51%)	H->L+1 (49%)
	339	0.22	H-3->L (23%)	H-2->L (21%), H-1->L+2 (14%), H-1->L (11%)
	338	0.16	H-2->L (20%)	H-3->L+1 (20%), H->L+2 (15%)
	331	0.04	H->L (29%)	H-1->L+1 (29%), H-3->L+1 (18%), H-2->L (13%)

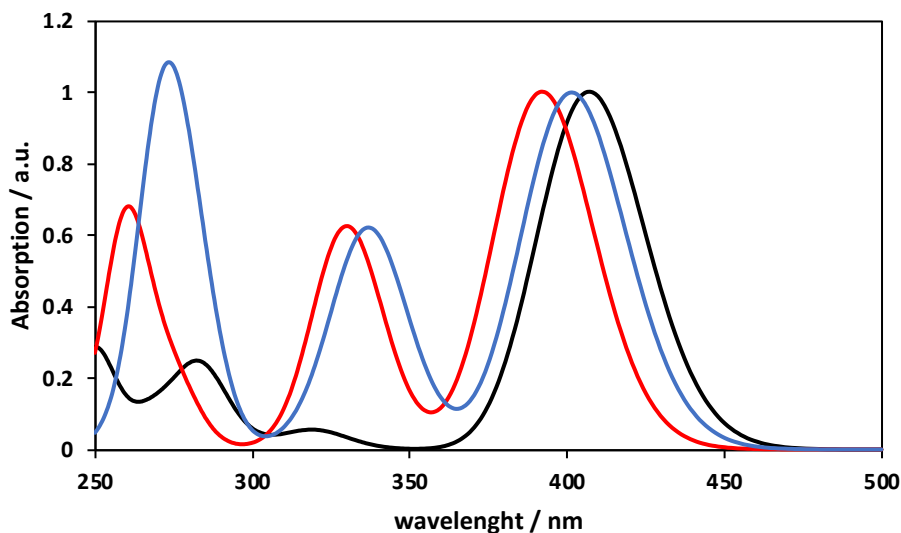


Figure S21. TD-DFT simulated absorption spectra of **BTI** (black curve), **TCI** (red curve) and **TCI₂** (blue curve). TD-DFT computed transitions were convoluted with gaussian functions having a FWHM of 0.3 eV.

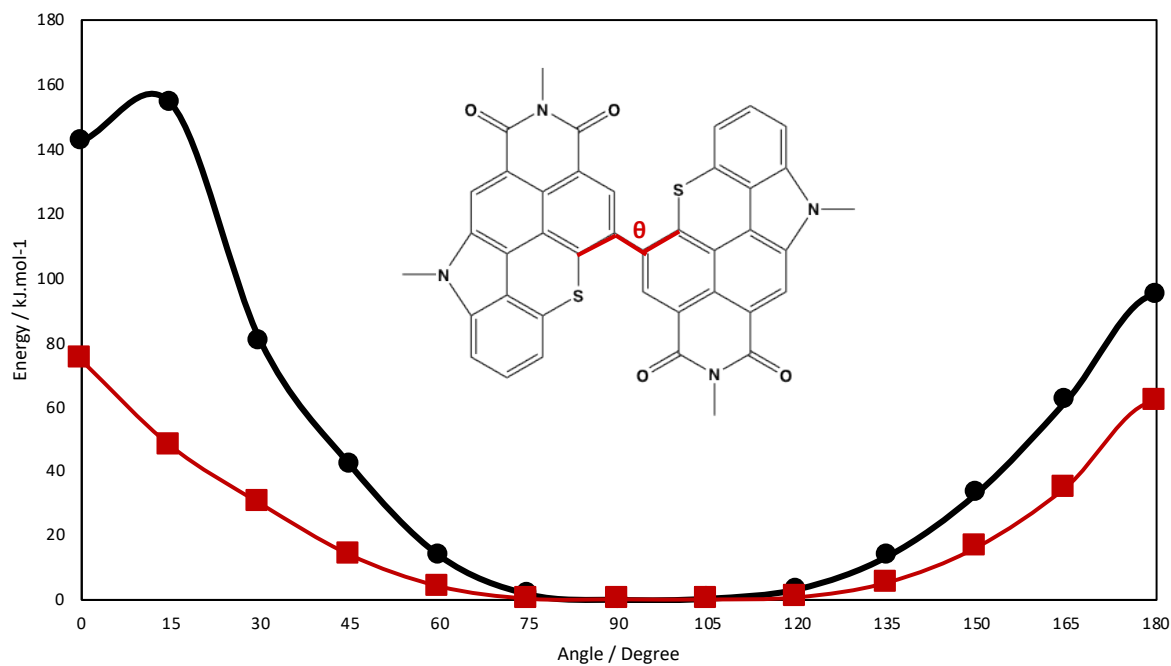


Figure S22. Computed potential energy surface along the dihedral angle of TCl_2 for the S_0 (black curve) and S_1 (red curve) states.

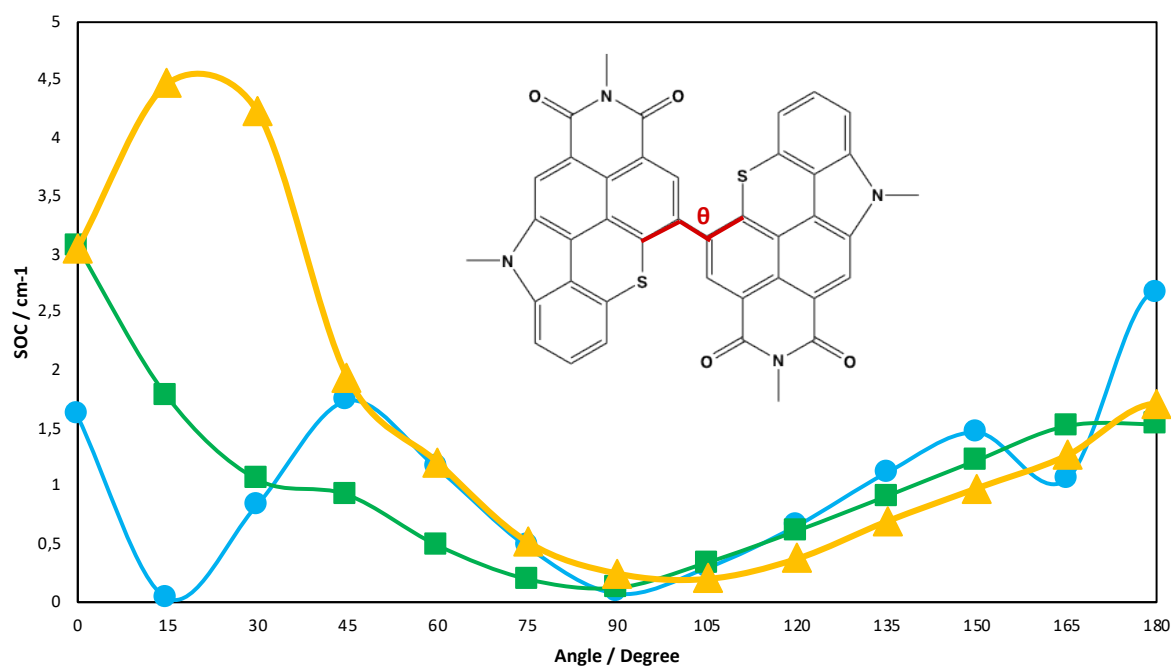


Figure S23. Computed SOC between S_1 and T_1 (blue curve), T_2 (green curve) and T_3 (yellow curve) as a function of the dihedral angle of the dimer.

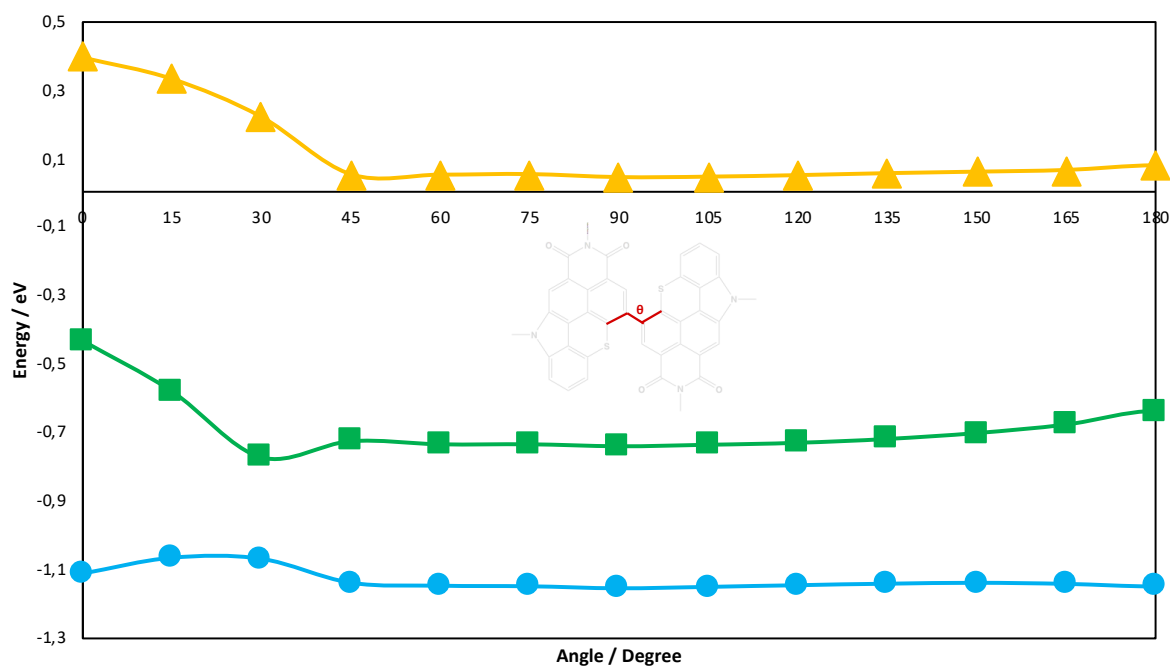


Figure S24. Computed T₁ (blue curve), T₂ (green curve) and T₃ (yellow curve) energies compared to S₁ (0 eV energy line) as a function of the dihedral angle of the dimer.

Device Fabrication and testing

Poly(9,9-di-n-octylfluorenyl-2,7-diyl) (PFO), o-xylene, methanol and PET substrates coated with transparent metal layer, indium-tin-oxide (ITO), were obtained from Millipore-Sigma. (Poly [(9,9-bis(3'-(N,N dimethylamino)propyl)-2,7-fluorene)-alt-2,7-(9,9-dioctylfluorene)]) (PFN) was purchased from Ossila Ltd. (Sheffield, UK). PEDOT:PSS dissolved in water was supplied from Heraeus (Hanau, Germany).

FOM nanoroll coater (from FOM Technologies, Copenhagen S., Denmark), a roll slot-die coater, was used for coating OLEDs layers on flexible PET substrates. Spin-coater from Ossila Ltd., Sheffield, UK, was used to form spin-coated OLED layers. The top silver layer as a cathode was deposited using M. Braun Inertgas-Systeme (GmbH, Garching, Germany) thermal evaporator.

The electrical measurements (current-voltage) were measured using the Keithley Source meter (Model: 2612B from Tektronix, Inc., Beaverton, USA). Luminance meter (model: LS 150, supplied from Konica Minolta, Inc., Tokyo, Japan) was used to obtain the Luminance of OLEDs.

OLEDs stack includes - Glass/ITO/PEDOT:PSS/ PFO:TCI₂/PFN/Ag. In the beginning, the ITO coated glass substrates were cleaned in an ultrasonic bath with acetone, propanol, and water for 5 min

each. After cleaning, the ITO surface was treated using UV ozone. Then, the PEDOT:PSS solution was spin-coated at 4000 rpm for 60 s and annealed at 150 °C for 30 min. The PEDOT:PSS solution was filtered with a 0.45 µm pore size PVDF filter before spin coating. On top of PEDOT:PSS, the light-emitting blend (PFO:TCl₂) solution was spin-coated, and the films were annealed at 90 °C for 30 min. The PFO and TCl₂ ratios were 19:1 with 15mg/ml of concentration in o-xylene. The PFN solution was spin-coated over an emissive layer at 5000 rpm for 60 s and dried at 90 °C for 30 min. The PFN solution consisted of 2 mg of PFN in 1 ml methanol and two µL of acetic acid. Finally, the silver was deposited through thermal evaporation.

Emitter	Turn-on Voltage (V)	Max. luminance (cd/m ²)	Max. Current efficiency (cd/A)	EQE (%)
TCl ₂	12	524	0.9	0.19
BTI ₂	9.9	608	0.3	0.04

Table S4 Comparison of the device performances of BTI₂ and TCl₂ on ITO based small area devices⁵

References

1. M. J. Frisch, G. W. Trucks, H. B. Schlegel, G. E. Scuseria, M. A. Robb, J. R. Cheeseman, G. Scalmani, V. Barone, G. A. Petersson, H. Nakatsuji, X. Li, M. Caricato, A. V. Marenich, J. Bloino, B. G. Janesko, R. Gomperts, B. Mennucci, H. P. Hratchian, J. V. Ortiz, A. F. Izmaylov, J. L. Sonnenberg, Williams, F. Ding, F. Lipparini, F. Egidi, J. Goings, B. Peng, A. Petrone, T. Henderson, D. Ranasinghe, V. G. Zakrzewski, J. Gao, N. Rega, G. Zheng, W. Liang, M. Hada, M. Ehara, K. Toyota, R. Fukuda, J. Hasegawa, M. Ishida, T. Nakajima, Y. Honda, O. Kitao, H. Nakai, T. Vreven, K. Throssell, J. A. Montgomery Jr., J. E. Peralta, F. Ogliaro, M. J. Bearpark, J. J. Heyd, E. N. Brothers, K. N. Kudin, V. N. Staroverov, T. A. Keith, R. Kobayashi, J. Normand, K. Raghavachari, A. P. Rendell, J. C. Burant, S. S. Iyengar, J. Tomasi, M. Cossi, J. M. Millam, M. Klene, C. Adamo, R. Cammi, J. W. Ochterski, R. L. Martin, K. Morokuma, O. Farkas, J. B. Foresman and D. J. Fox, *Journal*, 2016.
2. T. Yanai, D. P. Tew and N. C. Handy, *Chemical Physics Letters*, 2004, **393**, 51-57.
3. S. Grimme, S. Ehrlich and L. Goerigk, 2011, **32**, 1456-1465.
4. K. Aidas, C. Angeli, K. L. Bak, V. Bakken, R. Bast, L. Boman, O. Christiansen, R. Cimraglia, S. Coriani, P. Dahle, E. K. Dalskov, U. Ekström, T. Enevoldsen, J. J. Eriksen, P. Ettenhuber, B. Fernández, L. Ferrighi, H. Fliegl, L. Frediani, K. Hald, A. Halkier, C. Hättig, H. Heiberg, T. Helgaker, A. C. Hennum, H. Hettrema, E. Hjertenæs, S. Høst, I.-M. Høyvik, M. F. Iozzi, B. Jansík, H. J. A. Jensen, D. Jonsson, P. Jørgensen, J. Kauczor, S. Kirpekar, T. Kjærgaard, W. Klopper, S. Knecht, R. Kobayashi, H. Koch, J. Kongsted, A. Krapp, K. Kristensen, A. Ligabue, O. B. Lutnæs, J. I. Melo, K. V. Mikkelsen, R. H. Myhre, C. Neiss, C. B. Nielsen, P. Norman, J. Olsen, J. M. H. Olsen, A. Osted, M. J. Packer, F. Pawłowski, T. B. Pedersen, P. F. Provasi, S. Reine, Z. Rinkevicius, T. A. Ruden, K. Ruud, V. V. Rybkin, P. Sałek, C. C. M. Samson, A. S. de Merás, T. Saue, S. P. A. Sauer, B. Schimmelpfennig, K. Sneskov, A. H. Steindal, K. O. Sylvester-Hvid, P. R. Taylor, A. M. Teale, E. I. Tellgren, D. P. Tew, A. J. Thorvaldsen, L. Thøgersen, O. Vahtras, M. A. Watson, D. J. D. Wilson, M. Ziolkowski and H. Ågren, 2014, **4**, 269-284.

5. J. M. Andrés Castán, C. Dalinot, S. Dayneko, L. Abad Galan, P. Simón Marqués, O. Alévêque, M. Allain, O. Maury, L. Favereau, P. Blanchard, G. C. Welch and C. Cabanetos, *Chem. Commun.*, 2020, **56**, 10131-10134.